Metal Process Simulation Laboratory
Department of Mechanical and Industrial Engineering
University of Illinois at Urbana-Champaign
Urbana, IL 61801

Effect of Gas Bubble Size on Fluid Flow in Continuous Casting Mold

Tiebiao Shi and Brian G. Thomas

Continuous Casting Consortium

Report
2000

Submitted to

Allegheny Ludlum
AK Steel
Columbus Stainless
Inland Steel
LTV
Stollberg, Inc

March 21, 2000

Effect of gas bubble size on fluid flow in a continuous casting mold

1. Abstract

In this project, a 3-D gas-liquid multiphase turbulent flow model is developed for continuous casting. The standard K-ε turbulence model is used to solve turbulent flow equations. With this model, the effects of bubble size on liquid flow patterns, the formation of gas entrapment defects and the formation of inclusion particles are investigated. With increasing bubble size, liquid flow patterns change from single roll to double roll. Small bubbles (d<1.5mm) have larger tendency to be entrapped by the growing shell than do large bubbles. Small bubbles are more likely to entrap flux into the liquid than large bubble. Medium size bubbles (1.omm-2.0mm) are expected to have the largest possibility to have inclusion problems. The most likely position where inclusion problems happen is near the SEN. Although gas bubbles attach to inclusion particles and help to remove them, the simulation shows that flow with injecting gas might lead to more inclusion problems than flow without gas due to its entraining more flux, if the inlet liquid steel is clean.

2. Objectives

In this project, following problems will be investigated so that some clues to prevent defects could be extracted.

a) How bubble size affects flow patterns.

b) How bubble size affects gas entrapment.

c) How bubble size affects the formation of inclusions.

3. Background

Argon gas injection is a common practice in continuous casting. Argon gas is applied at several stages in the continuous casting process to encouraging mixing, to help prevent nozzle clogging, and to promote the flotation of solid inclusion particles from liquid steel. However, gas bubbles change flow pattern greatly[1, 2] and might bring in some new problems.

Bubble size is one of the major factors which influence flow pattern. B.G.Thomas[2] et al investigated the effects of bubble size on flow pattern and heat transfer and gained important results, but only considered two different bubble sizes and did not extend the work to predict defects.

In this study, three-dimensional models of fluid flow are developed using a commercial package CFX. Coupled liquid phase and gas phase equations are solved simultaneously. Seven different bubble sizes ranging from 0.5mm to 4.0mm are modeled . Gas volume fraction is set constant at 8.5%. Flow without gas is also modeled. The effects of bubble size on flow pattern and other parameters related to defect formation are investigated.

4. Model Description

4.1 Model description

The 3-D gas-liquid multiphase flow is modeled in this study . The standard K-ε turbulence model is used to solve this multiphase flow. A commercial software package CFX is used to simulate the standard K-ε turbulence model. User subroutine is written to set up a sink on top surface to absorb gas.

The liquid flow in the mold is turbulence flow. Standard K-ε model is used to solve turbulent flow. Only large scale, steady (time-invariant) turbulent eddies could be simulated in this model. The gas phase is assumed to be laminar. An Eulerian multiphase multi-fluid model is used to simulate the flow of gas bubbles in the liquid steel. Each phase has it's own velocity, K and ε fields. The pressure field is shared for the two phases. The velocity fields are coupled by an empirical inter-phase drag model.

The gas bubbles and particles concentrate mainly in upper liquid pool in the strand. To save computing time, the length of domain is set to 3m from meniscus. Considering the symmetry of the geometry, only one quarter of the strand is modeled. Fig.1 shows the schematic of simulation domain and boundary conditions for modeling. According to the work of D. Creech[3], it is reasonable to neglect the solidified shell in the modeling.

4.2 Governing Equations

Momentum equation for liquid phase:

$$\nabla \cdot (f_{liq}(\rho_{liq} V_{liq} \otimes V_{liq})) = \nabla(f_{liq}\mu_{eff}(\nabla V_{liq} + (\nabla V_{liq})^T)) - f_{liq}\nabla p + c_{drag}(V_{gas} - V_{liq}) + S_{liq}$$

Momentum equation for gas phase:

$$\nabla \cdot (f_{gas}(\rho_{gas} V_{gas} \otimes V_{gas})) = \nabla(f_{gas}\mu_{eff}(\nabla V_{gas} + (\nabla V_{gas})^T)) - f_{gas}\nabla p + c_{drag}(V_{liq} - V_{gas}) + S_{gas}$$

where f is volume fraction, V is velocity. p is pressure, S is the momentum source, subscript *liq* and *gas* are liquid and gas respectively.

Transport equations for liquid phase:

$$\nabla \cdot (f_{liq}(\rho_{liq} K_{liq} V_{liq})) = \nabla \cdot (f_{liq}(\mu_{liq} + \frac{\mu_{liq}}{\mathrm{Pr}_K})\nabla K_{liq}) + f_{liq}\Phi_{liq} - f_{liq}\rho_{liq}\varepsilon_{liq}$$

$$\nabla \cdot (f_{liq}(\rho_{liq} \varepsilon_{liq} V_{liq})) = \nabla \cdot (f_{liq}(\mu_{liq} + \frac{\mu_{liq}}{\mathrm{Pr}_\varepsilon})\nabla \varepsilon_{liq}) + C_1 f_{liq}\frac{\varepsilon_{liq}}{K_{liq}}\Phi_{liq} - C_2 f_{liq}\rho_{liq}\frac{\varepsilon^2{}_{liq}}{K_{liq}}$$

where Φ_{liq} is defined as

$$\Phi_{liq} = \mu_{liq_{eff}}\nabla V_{liq} \cdot (\nabla V_{liq} + (\nabla V_{liq})^T) - \frac{2}{3}\nabla \cdot V_{liq}(\mu_{liq_{eff}}\nabla V_{liq} + \rho_{liq}K_{liq})$$

Transport equations for gas phase:

$$\nabla \cdot (f_{gas}(\rho_{gas} K_{gas} V_{gas})) = \nabla \cdot (f_{gas}(\mu_{gas} + \frac{\mu_{liq}}{\mathrm{Pr}_K})\nabla K_{gas}) + f_{gas}\Phi_{gas} - f_{gas}\rho_{gas}\varepsilon_{gas}$$

$$\nabla \cdot (f_{gas}(\rho_{gas} \varepsilon_{gas} V_{gas})) = \nabla \cdot (f_{gas}(\mu_{gas} + \frac{\mu_{gas}}{\mathrm{Pr}_\varepsilon})\nabla \varepsilon_{gas}) + C_1 f_{gas}\frac{\varepsilon_{gas}}{K_{gas}}\Phi_{gas} - C_2 f_{gas}\rho_{gas}\frac{\varepsilon^2{}_{gas}}{K_{gas}}$$

where

$$\Phi_{gas} = \mu_{gas_{eff}}\nabla V_{gas} \cdot (\nabla V_{gas} + (\nabla V_{gas})^T) - \frac{2}{3}\nabla \cdot V_{gas}(\mu_{gas_{eff}}\nabla \cdot V_{gas} + \rho_{gas}K_{gas})$$

4.3 Boundary conditions

The schematic of simulation domain and boundary conditions is shown in Fig.1.

4.3.1 Narrow face, wide face and top surface

These faces are set non-slip wall conditions (V_x=V_y=V_z=0). In the standard K-ε model, wall law is applied to these walls. Many of variables vary rapidly in the near-wall regions of the flow. Instead of using extremely fine grids in this region, empirical wall functions

are used to specify flow behavior. This allows coarser grids used and still have good specification of flow behavior in the boundary layer.

In standard K-ε model, tangential velocity to the wall is calculated as:

The non-dimensional distance normal to the wall

$$y^+ = \frac{(\rho^2 C_\mu{}^{1/2} K)^{1/2}}{\mu} n$$

The tangential velocity

$$V_t = \begin{cases} -(C_\mu K)^{1/2} y^+ & y^+ < y_0^+ \\ \dfrac{-(C_\mu K)^{1/2}}{\kappa} \log(E y^+) & y^+ \geq y_0^+ \end{cases}$$

where V_t is the tangential velocity to the wall, C_μ is a turbulence model constant. K is turbulence kinetic energy. μ is viscosity. *n* is normal distance to the wall. E is log-layer constant. κ is the Von-Karmen constant.

4.3.2 Nozzle port

The nozzle port is the inlet boundary where velocity, K, and ε are specified. The pressure gradient is left equal to zero, so inlet pressures are extrapolated from downstream.

4.3.3 Bottom of domain

The bottom of domain is set to a pressure boundary. Previous work showed that the pressure boundary condition can handle outlets where flow is not fully developed better than the mass flow boundary[4]. Zero pressure is specified. Zero normal gradient boundary conditions are specified on other variables.

4.3.4 Two symmetry planes

The two symmetry planes have velocity normal to the plane set to zero. For all other variables, including pressure, zero normal gradient boundary conditions are specified.

5. Model validation and scaling

5.1 Model validation

D.Creech's [3] used this model to simulate P.Andrzejewski[7] etc's experiments. The comparison between simulation and experimental measurements is shown in Fig.2. The predicted flow patterns match experiments reasonably well.

Fig. 3 compares the flow patterns of the PIV water model measurements [8] and simulation results by this model. Fig.4 compares average speed along the jets of the PIV measurement and simulation result of this model. The simulation matches the PIV measurement very well.

The vertical velocity of bubbles relative to the liquid can be compared with analytical calculations of floating velocity of bubbles in stagnant liquid to tell whether or not the modeling reasonably describes the movement of bubbles. Table 1 compares analytical calculations of floating velocity of bubbles in stagnant liquid and relative vertical velocity of bubbles with liquid from the CFX model. The reason of the large difference might be that bubbles don't reach its steady velocity due to the short distance from nozzle port to meniscus while floating velocity of bubbles is calculated by assuming bubbles reach a steady velocity. However, both analytical calculation and modeling show the same tendency of changing velocity with bubble size.

Table.1 Comparison between analytical value and CFX simulation result of vertical velocity

Bubble Diameter (mm)	Drag force $F=V(\rho-\rho')g$	Bubble floating speed in stagnant liquid steel $F=6\pi\mu R*V_z$ (m/s)	Average difference between V_{zl} and V_{zg} (m/s)
0.5	3.69×10^{-5}	0.699	0.0552
0.7	1.01×10^{-4}	1.37	0.0787
1.0	2.96×10^{-4}	2.80	0.110
1.5	9.98×10^{-4}	6.3	0.170
2.0	2.36×10^{-3}	11.2	0.207
3.0	7.98×10^{-3}	25.2	0.290
4.0	1.89×10^{-2}	44.8	0.336

* CFX simulation data of vertical velocity is taken along the horizontal line 10 mm below meniscus in the wide centerplane.

5.2 Scaling

Let's scale momentum equation in x direction:

$$\rho_{liq}(\frac{\partial V_x}{\partial t}+V_x\frac{\partial V_x}{\partial x}+V_y\frac{\partial V_x}{\partial y}+V_z\frac{\partial V_x}{\partial z})=-\frac{\partial P}{\partial x}+\mu(\frac{\partial^2 V_x}{\partial x^2}+\frac{\partial^2 V_x}{\partial y^2}+\frac{\partial^2 V_x}{\partial z^2})$$

Assume a time interval t_c, $t^*=\frac{t}{t_c}$

Other variables are scaled as:

$$x^*=\frac{x}{L_z}\ ,\ y^*=\frac{y}{L_z}\ ,\ z^*=\frac{z}{L_z}\ ,\ V_x^*=\frac{V_x}{V}\ ,\ P^*=\frac{P}{P_{\max}}$$

Here L_z is the distance from top surface to exit of domain. V is the inlet velocity.

The scaled momentum equation is like below:

$$\rho_{liq}(\frac{V}{t_c}\frac{\partial V_x^*}{\partial t^*}+\frac{V^2}{L_z}V_x^*\frac{\partial V_x^*}{\partial x^*}+\frac{V^2}{L_z}V_y^*\frac{\partial V_x^*}{\partial y^*}+\frac{V^2}{L_z}V_z^*\frac{\partial V_x^*}{\partial z^*})=-\frac{P_{\max}}{L_z}\frac{\partial P^*}{\partial x^*}+\mu\frac{V}{L_z{}^2}(\frac{\partial^2 V_x^*}{\partial x^{*2}}+\frac{\partial^2 V_x^*}{\partial y^{*2}}+\frac{\partial^2 V_x^*}{\partial z^{*2}})$$

Because pressure change along x direction is small, $\frac{\partial P^*}{\partial x^*}\to 0$.

Rearranging above equation:

$$\frac{\rho_{liq}L_z}{Vt_c}\frac{\partial V_x^*}{\partial t^*}+V_x^*\frac{\partial V_x^*}{\partial x^*}+V_y^*\frac{\partial V_x^*}{\partial y^*}+V_z^*\frac{\partial V_x^*}{\partial z^*}=\frac{\mu}{\rho_{liq}VL_z}(\frac{\partial^2 V_x^*}{\partial x^{*2}}+\frac{\partial^2 V_x^*}{\partial y^{*2}}+\frac{\partial^2 V_x^*}{\partial z^{*2}})$$

From above equation, we can have such conclusions:

1) When t_c is large, for example 1hour, the turbulent term $\frac{\partial V_x^*}{\partial t^*}$ becomes small. This means the flow becomes stable when it is investigated during a long time. When t_c is small, turbulent character of the flow is greater.

2) $\frac{1}{\mathrm{Re}}=\frac{\mu}{\rho_{liq}VL_z}=\frac{5.55\times10^{-3}}{7020\times2.5\times3}=1.05\times10^{-7}$

This means turbulent character of the flow is mainly decided by fluid inertia terms. The viscous terms have little contribute to the turbulent character of the flow.

6. Results and Analysis

6.1 Effect of bubble size on flow pattern

Gas injection affects the casting process through its influence on the liquid flow pattern. The extent of this effect depends on factors such as the gas injection rate, the bubble size, jet velocity etc. In this study, all variables are fixed except bubble size. Mean bubble diameter changes from 0.5mm to 4.0mm, which covers the bubble size range met in practice. The effect of bubble size on the flow pattern is shown in Fig. 5. Small bubbles (d<1.5mm) have greater influence on the liquid flow than big bubbles (d>1.5mm). They tend to stay with the flowing jet longer and bend it upward to impinge the top surface. Only a single roll pattern forms. Big bubbles tend to float up faster and split the jet. In this case, the jets divide into two branches of flow. One branch floats up quickly when the jet enters the domain and impinges the top surface. Another flow, which has little gas left with it, moves on and impinges the narrow face. A double roll flow pattern is formed by the lower jet. For the non-gas case, the jet moves directly across the mold cavity and forms a double roll flow pattern after impinging the narrow face.

6.2 Effect of bubble size on gas entrapment

Most gas bubbles float upward to escape from the top surface due to the strong buoyancy force. Bubbles entering the lower circulation zone have a larger chance to be trapped. Although no more than 5% gas enters lower circulation zone of the liquid flow [2], it is still dangerous if these bubbles cannot escape because even a tiny volume fraction of gas trapped (as low as 10^{-4}% [5]) is very detrimental. Thus, to understand how and where bubbles are trapped, it is useful to examine how much gas enters the lower region of the mold and where the gas fraction is greater than 10^{-4}%.

The parameter “penetration depth” is used to indicate how deep the dangerous gas fraction level can extend below the meniscus. Penetration depth is defined as the deepest distance from the meniscus where the 10^{-5}% gas volume fraction contour reaches. It is assumed that the deeper the penetration depth, the more difficult it is for gas to float up to meniscus and the more likely it is for gas to be entrapped. This parameter gives a clue of how great is the chance that gas is trapped.

Fig.6 shows the penetration depth of different bubbles. For small bubbles (0.5mm ~ 1.0mm in diameter), the penetration depth increases with bubble size. In this size range, bubbles stay with the liquid steel flow. The smaller the bubble, the stronger its tendency

is to stay with the flow. Most of the flow will reach the top surface and let the gas escape (assuming there is not much resistance to entering the slag layer). With increasing bubble size, the total drag force between the bubbles and the liquid decreases. Some of flow will not be bend upward as much to meet the top surface. This part of the flow will stay down and have a deeper penetration. 1.0mm bubble has deepest penetration.

Large bubbles (1.5mm~4.0mm in diameter) have shallower penetration. Big bubbles have a smaller total surface area and thus impart a smaller drag force to the liquid steel flow. Most bubbles leave the jet quickly after entering domain. Very little gas goes down into the domain with the flow.

For large bubbles, the gas percentage near the narrow face is much smaller than 10^{-4}% (see Fig.7). This indicates that there is very small chance for large bubbles (1.5mm~4.0mm in diameter) to be trapped and form pencil-pipe defects on the narrow face.

Another parameter should be concerned is the area which is encloses by 10^{-05}% gas fraction contour on the solidifying shell. It is reasonable to assume that the larger this area is, the higher the likelyhood that bubbles are entrapped. Fig.8 shows the area enclosed by 10^{-05}% gas fraction contour for different bubbles. Small bubbles (0.5mm ~ 1.0mm) have much larger area enclosed by 10^{-05}% gas fraction contour than large bubbles (1.5mm~4.0mm). 1.0mm bubble has largest area. This indicates that small bubbles (especially around 1.0mm) are more prone to gas entrapment. Large bubbles (2.0mm~4.0mm) have very small such area and might not have gas entrapment.

It is assumed gas entrapment happens when the speed of gas flowing down the growing shell approaches the casting speed. It is much more possible for gas to be entrapped when the gas volume fraction is over 10^{-05}% and the gas downward velocity is close to casting speed simultaneously. Fig.9 shows the overlap of 10^{-05}% gas fraction contour and gas vertical velocity contour for four different bubbles. The red-shaded area is the overlap region. These regions might be the position where bubbles are most likely to be entrapped.

6.3 Effect of bubble size on inclusion entrapment

There are two major sources of inclusion particles: inclusion particles existing in inlet flow and inclusion particles sheared off from flux layer and entrapped into the flow. The first kind of inclusion particles comes from remaining particles produced in steel making

and erosion of refractory materials. Most of these particles circulate in the liquid pool and become entrained into the flux layer. Some of them are entrapped in the growing shell and initiate quality problems such as surface slivers. According to experiments by R.C.Sussman etc.[6], 22.3% of particles will not float up and finally remain in the solidified shell when gas is not injected into inlet flow. With such a high percentage of entrapment of particles, inclusion defects should be very common in continuous casting. Fortunately, this is not the case. Inclusion defects of happen only occasionally. This indicates that either alumina particles are infrequent in the inlet flow or that they are usually too small to cause a problem by themselves.

Flux particles sheared away and entrapped by liquid steel flow might be the major source of inclusion particles. There are two possible mechanisms by which flux is sheared away and entrained in the steel. The first mechanism is that flux could be sheared away by liquid level fluctuation on the interface of liquid steel and flux layer (Fig.10). The second is that flux also could be sheared by downward steel flow by the way as shown in Fig. 11. In the first mechanism, level fluctuation is the key parameter. In the second mechanism, the downward velocity near growing shell is the key parameter.

6.3.1. Effect of bubble size on level fluctuations

In CFX, turbulence is assumed isotropic. The average fluctuation velocity can be obtained by

Kinetic Energy K:

$$K = \frac{3}{2}\overline{u^2}$$

The level fluctuation height may be:

$$h = \frac{\rho_{steel} * K}{0.5(\rho_{steel} - \rho_{flux})g}$$

Fig.12 shows the maximum kinetic energy and maximum level fluctuations on the top surface for different bubble sizes. Generally, small bubbles have higher level fluctuation than larger bubbles. Flow without gas has smallest level fluctuation on the top surface. This suggest that small bubbles, while possibly having better cleaning effect on ermoving the small inclusion particles carried with the inlet flow, also have a higher tendency to entrain flux particles from the top flux layer. The particles entrapped by this way should have size smaller than 4.0mm in diameter.

6.3.2 Effect of bubble size on downward velocity near solidifying shell

During the operation of a continuous caster, the top liquid steel level is always moving up and down with fluctuation of inlet flow rate and casting speed. This might cause liquid steel level lower than the top of solidified shell sometimes. The top edge of the solidified shell may sometimes penetrate the flux layer like a blade. When the flux moves to the gap, the lower part of the flux layer is peeled off and stays at the solidified shell. If liquid steel flow is upward, the peeled flux would be put back and has less chance to form inclusion particles. Otherwise, the peeled flux would be pushed down into the liquid pool and form large inclusion particles. Because these particles form just near the growing shell, they are easily entrapped by the shell.

The maximum downward velocity at the meniscus indicates the tendency to entrap flux particles by this mechanism. Fig. 13 shows the effect of bubble size on vertical velocity around the top surface perimeter of mold. The maximum downward vertical velocity appears on the wide face in all eight cases. This indicates that the wide face might suffer more inclusion defects than the narrow face for these conditions via this mechanism. The position where inclusion particles concentrate is near the SEN on the wide face with a shallow depth. The maximum downward vertical velocity increases with increasing bubble size and reaches a maximum value for 1.5 mm bubbles. Then, it decreases with further increasing of bubble size. Bubbles between 1.0mm and 2.0mm have the largest maximum downward vertical velocity and might have largest tendency to suffer inclusion defects.

It should be noticed that flow without gas has much smaller vertical velocity around the top surface perimeter of the mold (than flow with gas). Considering that flow without gas also has the smallest level fluctuations, it suggests that flow without gas should have less inclusion defects than flow with gas in case that liquid steel is clean. If this is the case, we should find more flux inclusions in gas injection practice than in no gas practice.

7. Conclusions

1) The jet without gas goes straight forward and remains a single jet before it impinges on the narrow face. Jets with small gas bubbles (<1.5mm) bend upward and impinge on the top surface. Jets with large gas bubbles (>1.5mm) split into two branches. One, most of which is gas, goes up and impinges on the top surface. Another, most of which is liquid steel, goes forward and impinges on the narrow face. Both no gas flow

and flow with large bubbles (>1.5mm) show double roll flow pattern. Flow with small bubbles (<1.5mm) shows only a single roll flow pattern.

2) Medium size bubbles (around 1.0mm) appear to have the largest tendency to be entrapped. Smaller bubbles are less likely to slow down enough to be entrapped, while larger bubbles rarely go deep enough.

3) Smaller bubbles induce larger level fluctuation on top surface and increase the possibility of entrapping flux particles as inclusions into the solidifying meniscus.

4) Downward velocity along the solidified shell at the meniscus increases with increasing bubble size and reaches its maximum value for 1.5mm bubbles. Then it will decrease quickly. Bubble sizes between 1.0mm and 2.0mm have a greater chance to entrap flux particles in the growing shell.

5) Compared with flow with gas, flow without gas appears to have less likelyhood of entrapping flux particles, especially if the liquid steel is clean.

8. Implementation

1) Model has been developed to study multiphase flow in the mold. It is ready to simulate other cases and to optimize mold flow to minimize defects.
2) The modeling results in this project might help to understand the formation of some defects better and provide method to eliminate these defects.

9. Future Work

1) Some work is needed to do to give more accurate results near the wall so that the position of gas entrapment can be determined.
2) The effect of mixing of different size bubbles should be investigated so that the bubble size range in the plant can be identified.
3) Experiments should be done and evidence should be collected so that it becomes clear whether or not the suggestions here are correct. For example, does clean steel cast without gas have fewer inclusion problems than with gas (assuming aspiration in the nozzle is not a problem).

10. Acknowledgements

The authors wish to thank D.Creech for the model which is the basis of this work. LTV steel Corp. is acknowledged for PIV water model measurements. Thanks are also due to National Center for supercomputing Applications at University of Illinois for using computing facilities.

11. Reference

1. N.Bessho, R.Yoda and H.Yamasaki, Iron and Steelmaker,1991, vol. 18(4), pp.39-44.
2. B. G. Thomas and X. Huang , 76th Steelmaking Conference, Dallas, TX, March 28-31, 1993, Iron and Steel Society, Warrendale, PA, Vol.76, 1993, pp. 273-289.
3. D. Creech and B.G. Thomas, Continuous Casting Consortium Report, January 4, 1999.
4. H.Bai and B.G. Thomas, Annual Report, Continuous Casting Consortium, 1998
5. Y.Shang, Annual Report, Continuous Casting Consortium, 1996
6. R.C. Sussman , M.T. Burns , X. Huang and B.G. Thomas, 10th Process Technology Conference Proceedings, Toronto, Ontario, April 5-8,1992, Iron and Steel Society, Warrendale, PA, 1992,pp. 291-304.
7. P. Andrzejewski, K.U. Kohler and W. Pluscheli, Steel Research, 63(6), 1992, pp242-246.
8. Sivaramakrishnan, S., H. Bai, B.G. Thomas, P. Vanka, P. Dauby and M. Assar, "Transient Flow Structures in Continuous Cast Steel", *83rd Steelmaking Conference Proceedings*, (Pittsburgh, PA, March 26-29, 2000), Vol. 83, Iron and Steel Society, Warrendale, PA, 2000, 17p.

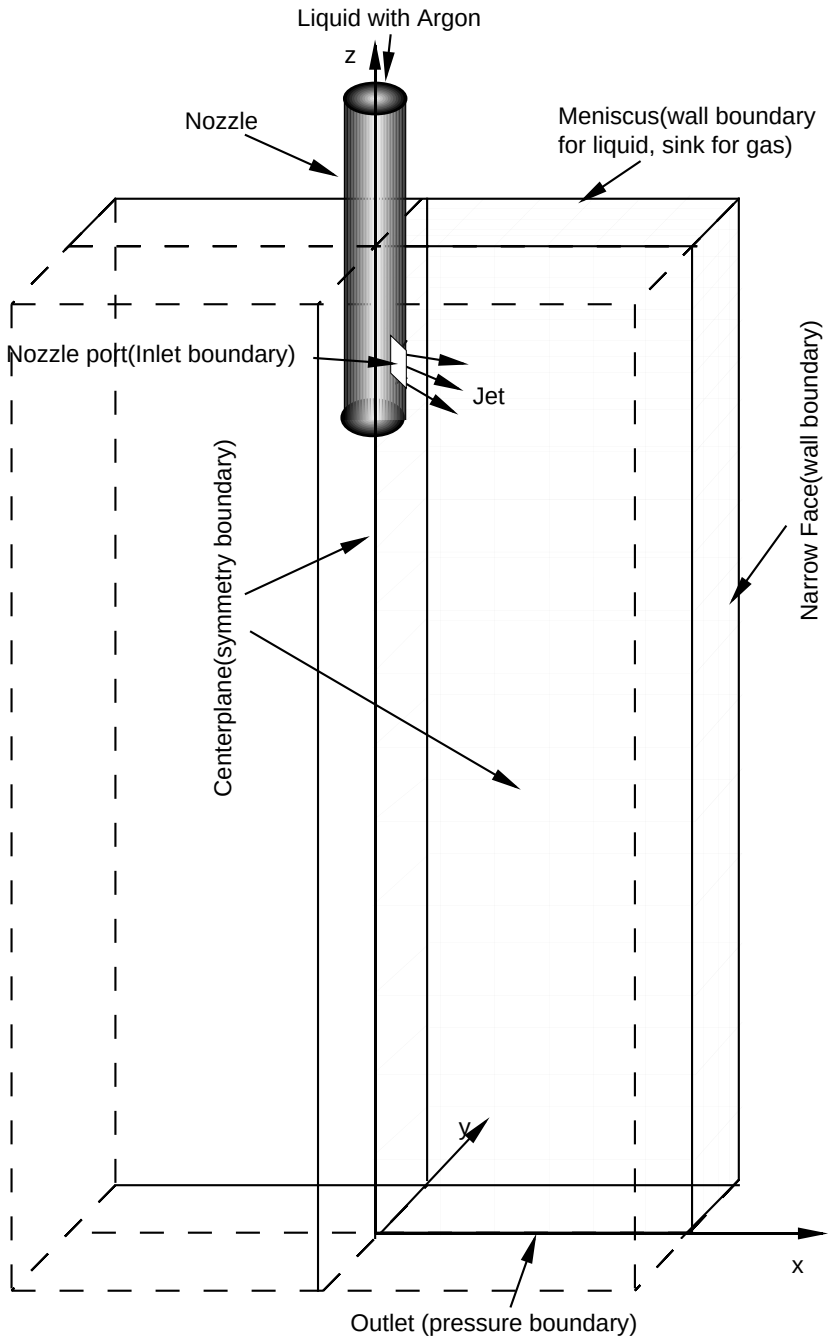

Fig.1 Shematic of simulation domain and boundary conditions

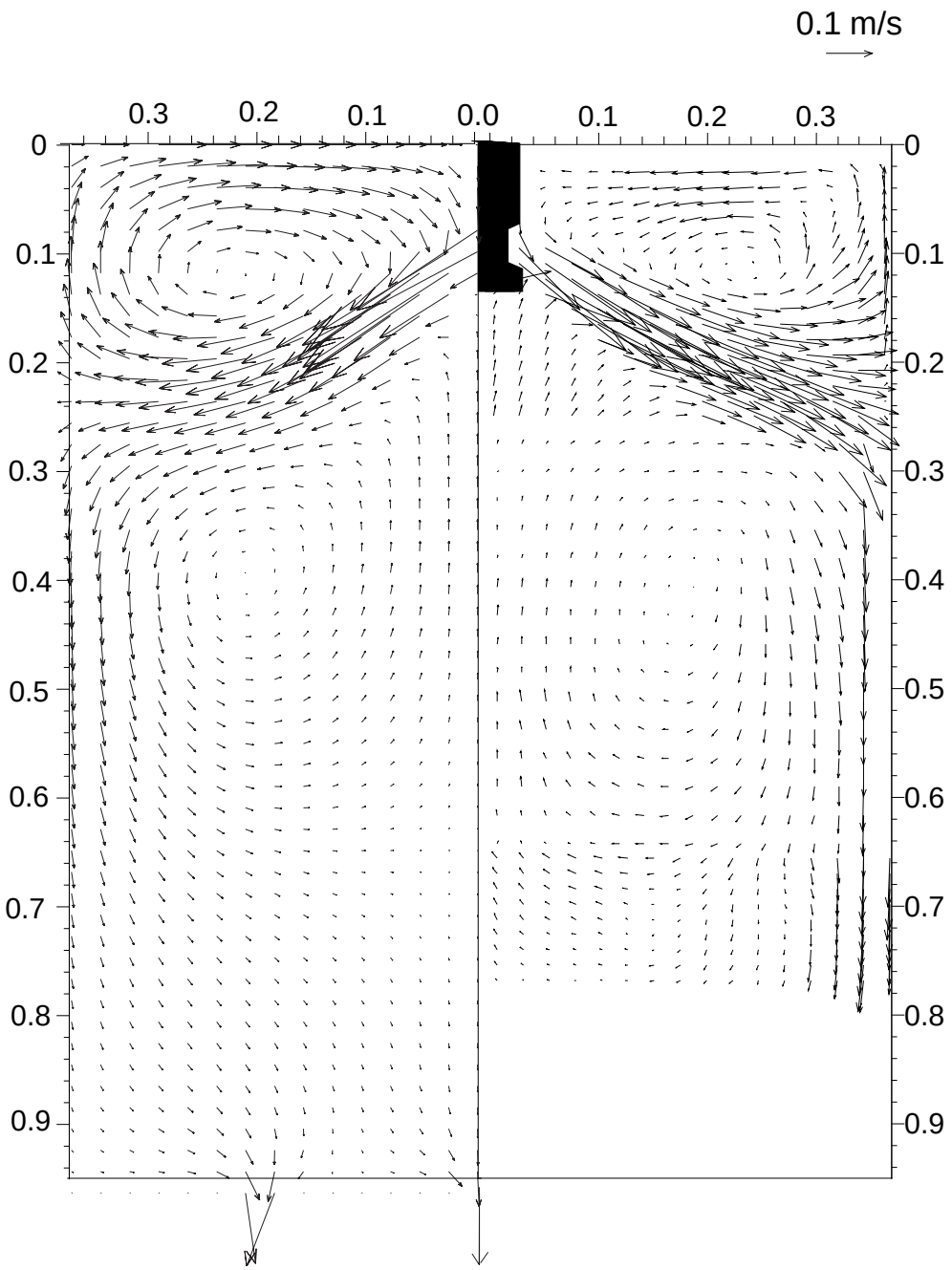

Left : Simulation Result Right : PIV Measurement

Fig.3 Comparison of Flow Patterns between PIV Measurements and Simulation

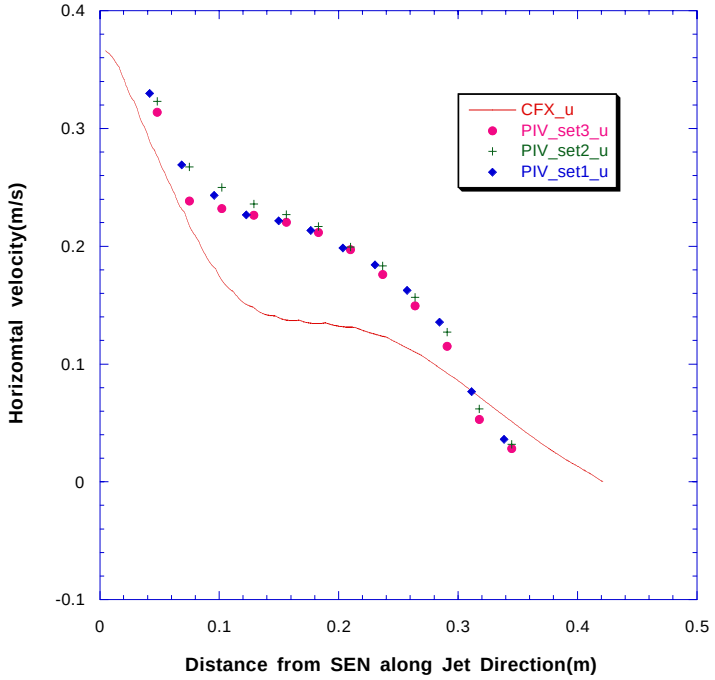

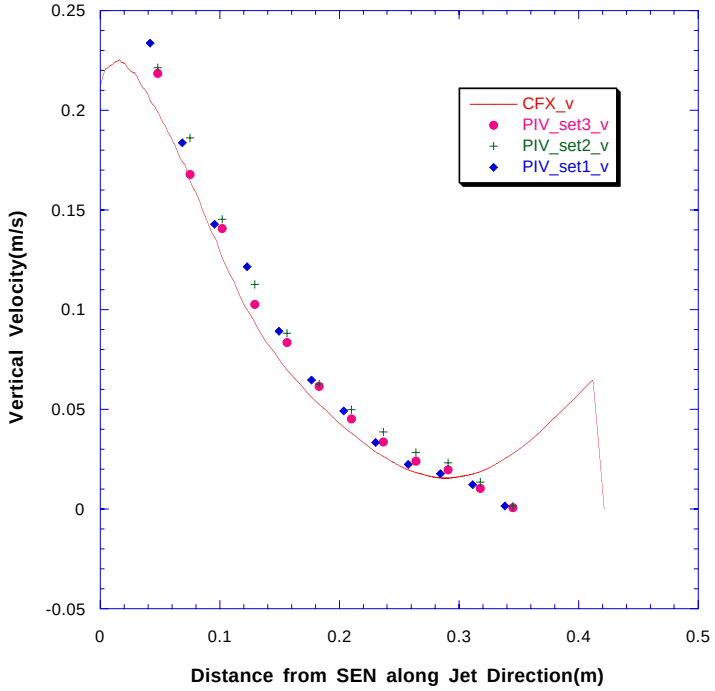

Fig.4 Comparison of Simulation Velocity along Jet With PIV Measurements

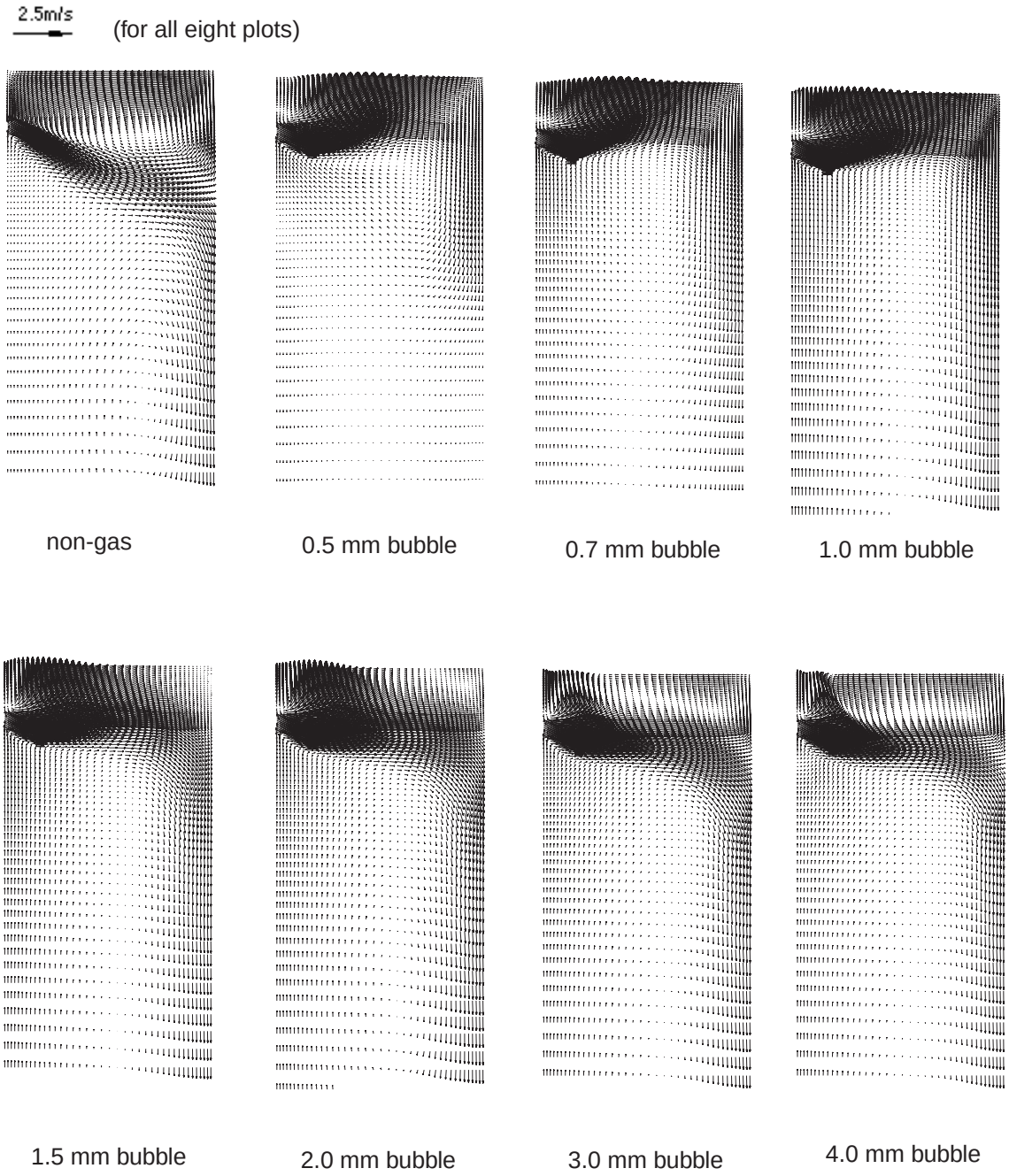

Fig.5 Effects of bubble size on fluid flow pattern in continuous casting mold

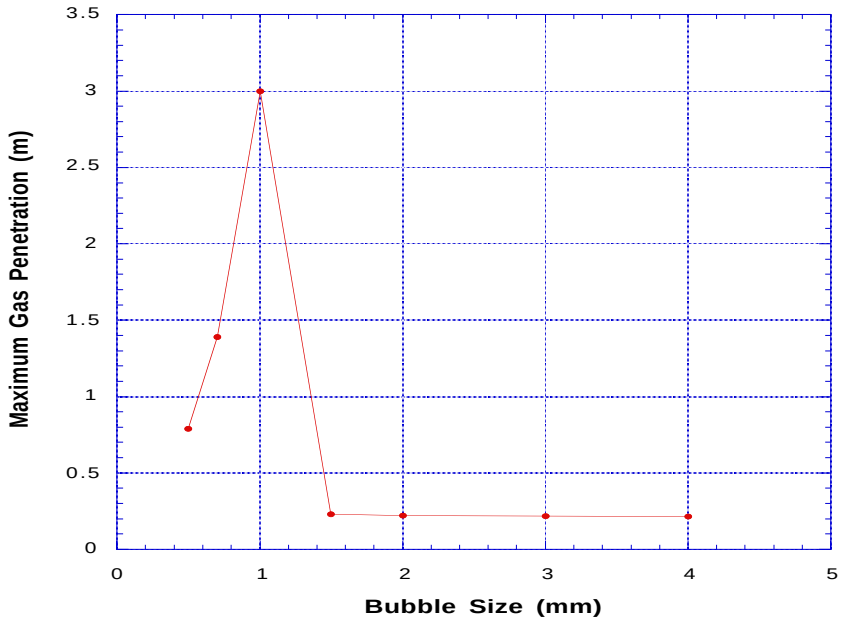

Fig.6 Effect of bubble size on gas penetration depth

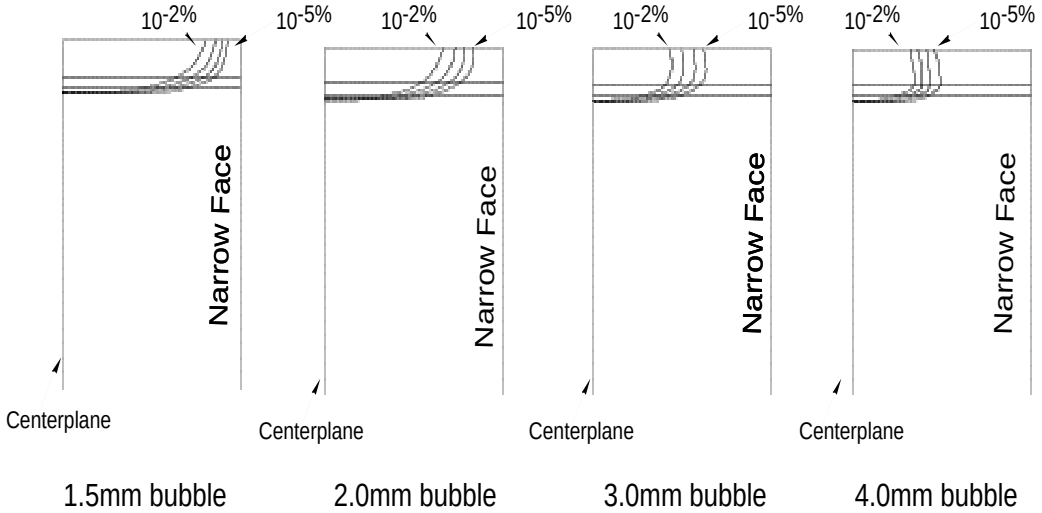

Fig.7 Gas Fraction Contour for Different sized Bubbles

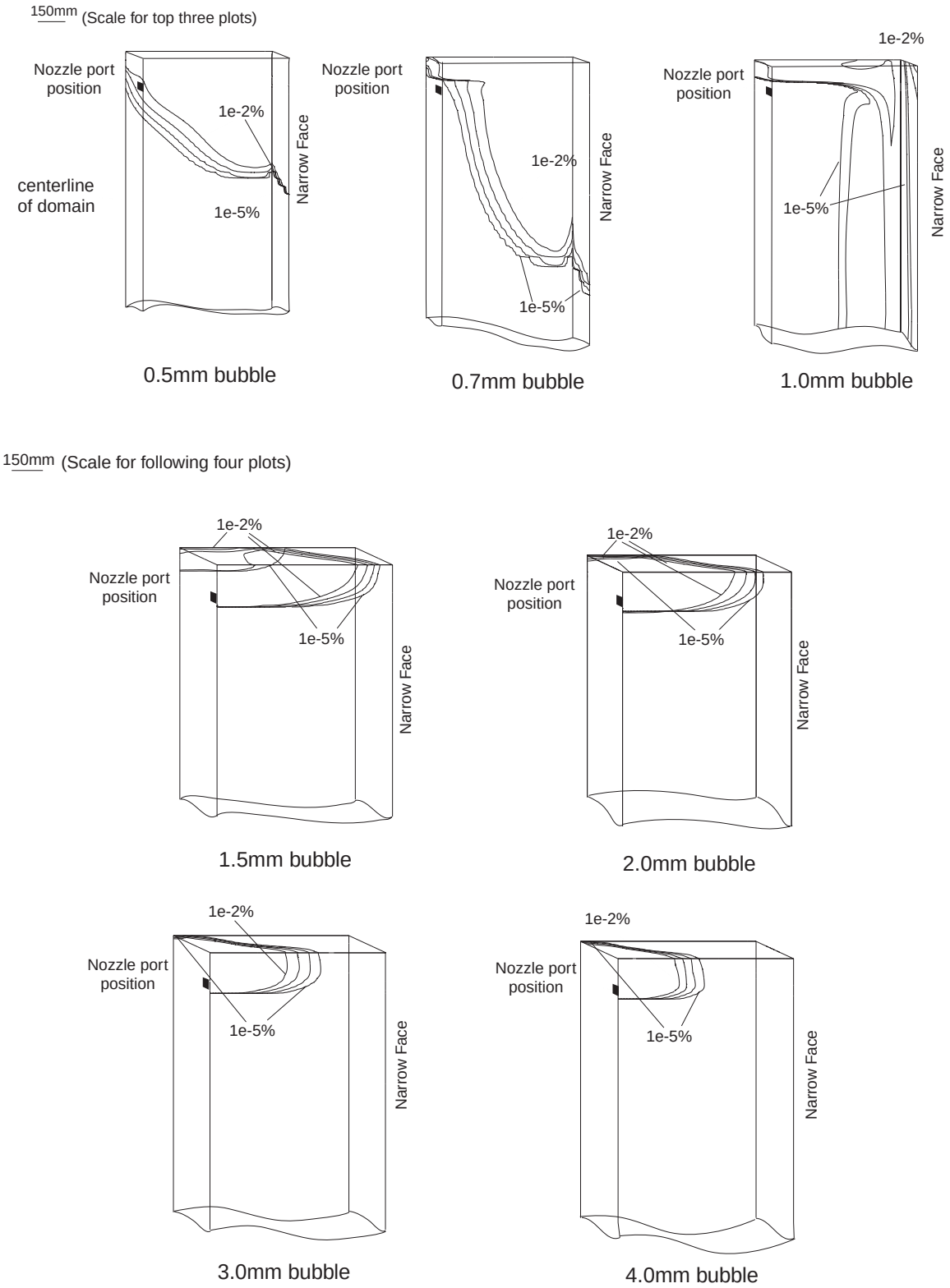

Fig.8 Gas percentage contour for different bubbles

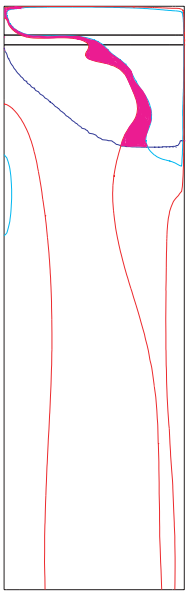

0.5 mm bubble

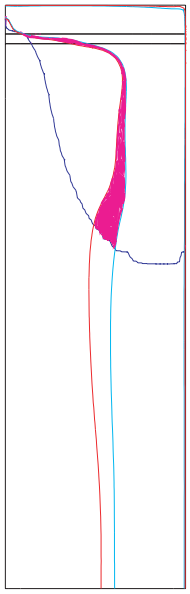

0.7 mm bubble

Explanations:

red line: W=-24mm/s contour

cyan line: W=-8mm/s contour

casting Speed = -14.8 mm/s

blue line:
1e-05% gas fraction contour

pink area:
The region where inclusions might occur

* All 4 pots are the planes 3mm offset wide face wall

1.0 mm bobble

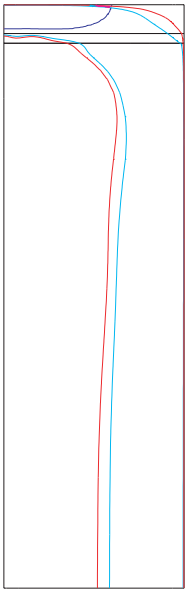

1.5 mm bubble

*The two horizontal line in the planes show the position of upper and lower boundary of the nozzle port

Overlap of the contours of gas fraction and vertical velocity

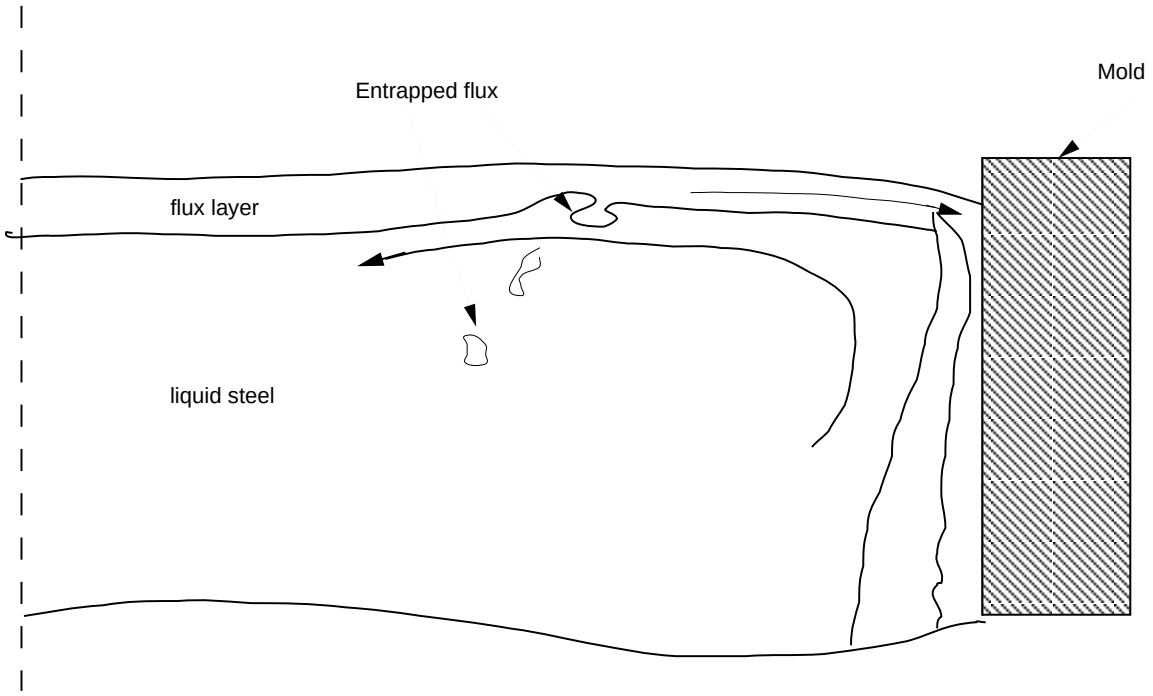

Fig 10. The first possible mechanism of entrapment of flux

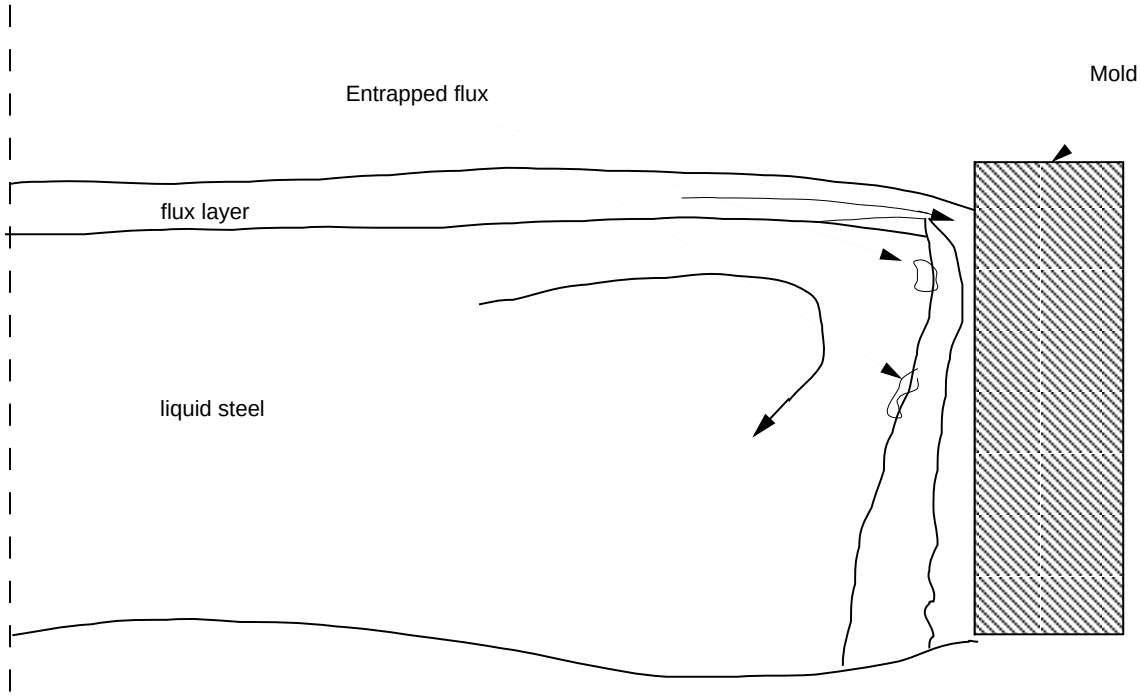

Fig 11. The second possible mechanism of entrapment of flux

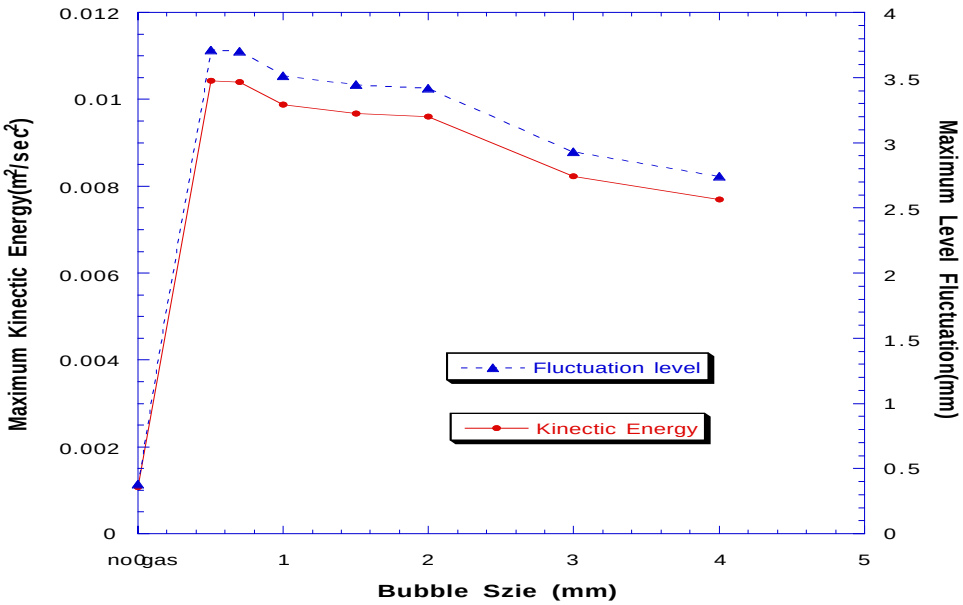

Fig. 12 Effect of bubble size on the maximum kinetic energy and level fluctuation on the top surface

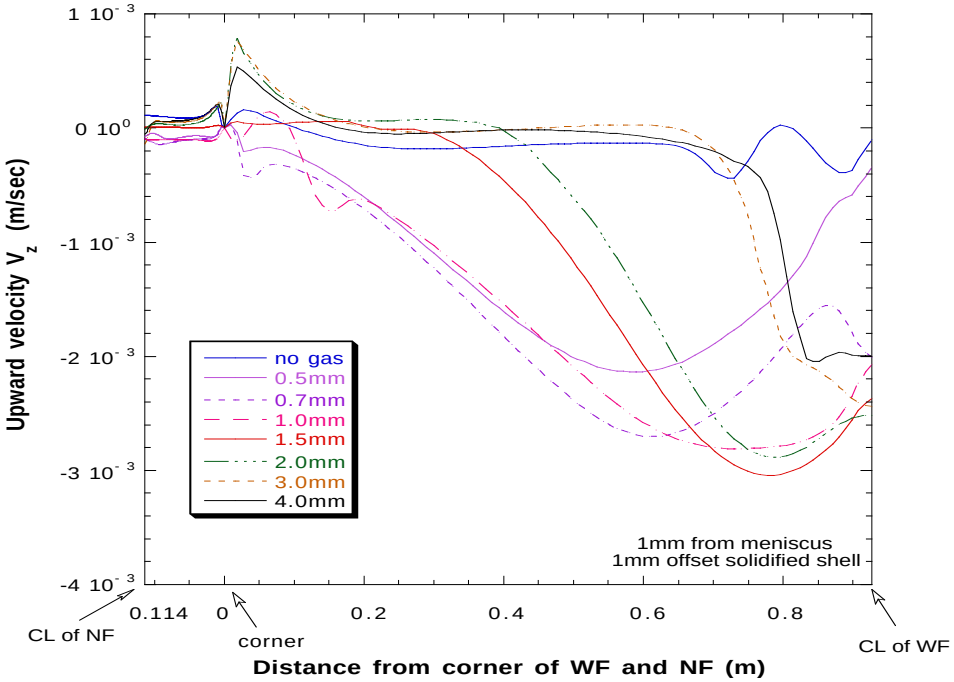

Fig.13 Effect of bubble size on vertical velocity around top surface perimeter